DOI: 10.1515/adms-2017-0019

Z. Ławrynowicz

University of Science and Technology UTP, Mechanical Engineering Faculty, Department of Materials Science and Engineering, Av. Kaliskiego 7, 85-796 Bydgoszcz, Poland
lawry@utp.edu.pl

BAINITIC REACTION AND MICROSTRUCTURE EVOLUTION IN TWO NORMALIZED AND TEMPERED STEELS DESIGNED FOR SERVICE AT ELEVATED TEMPERATURES

ABSTRACT

In the present work conventional heat treatment like normalizing (bainitic microstructure) and tempering of the alloys has been performed. The materials used in this study were two steels, one the laboratory prepared experimental low alloy Cr-Mo steel in comparison to typical commercial 10CrMo9-10 steel. The determined carbon concentrations of the residual austenite at the different temperatures of bainite transformation supports the hypothesis that the growth of bainitic ferrite occurs without any diffusion with carbon being partitioned subsequently into the residual austenite. It was found that bainitic reaction has stopped when average carbon concentration of the untransformed austenite is close to the T_0 line and supports formation of bainitic ferrite by a shear mechanism, since diffusionless transformation is not possible beyond the T_0 curve.

Normalized samples were air cooled down to room temperature before tempering at various temperatures in the range of 500-750^{o}C. Samples have been austenitized at 980^{o}C for 0.5 hour air cooled and tempered at 500, 550, 600, 650, 700 and 750^{o}C for 1 hour. After heat treatment, the assessment in the microstructure and phase precipitation was made using the samples prepared for metallographic and transmission electron microscope (TEM) on thin foils analysis. Quantitative X-ray analysis was used to determine the retained austenite content after heat treatment like normalizing and tempering and the total volume fraction of the retained austenite was measured from the integral intensity of the $(111)_\gamma$ and $(011)_\alpha$ peaks.

The changes observed in the microstructure of the steel tempered at the higher temperature, i.e. 750°C were more advanced than those observed at the temperature of 500°C. Performed microstructural investigations have shown that the degradation of the microstructure of the examined steel was mostly connected with the processes of recovery and polygonization of the matrix, disappearance of lath bainitic microstructure, the growth of the size of $M_{23}C_6$ carbides, and precipitation of the secondary M_2C precipitates. The magnitude of these changes depended on the temperature of tempering.

Keywords: *bainitic microstructure, normalizing, tempering, elevated temperatures, carbide precipitation*

INTRODUCTION

The Cr-Mo based low alloy steels are widely used in thermal power plants because of their ability to withstand elevated temperatures and high pressure under continuous service. Typically Cr-Mo steels are intended for boiler tubes, wire pairs, parts of boilers and steam turbines, components and other equipment operating at temperatures up to 580^o C [1].

The first Cr-Mo steels were used for conventional power-generation applications in the 1920s. The 2¼Cr-1Mo (nominally Fe-2.25Cr-1.0Mo-0.3Si-0.45Mn-0.12C) steel, designated

by ASTM as Grade 22, was introduced in the 1940s and is still widely used today. The next generation of heat-resistant steels, in addition to increased chromium, involved primarily the addition of the carbide formers vanadium and niobium to chemical compositions (i.e. T22 steel) to add precipitate strengthening and in some cases, a small molybdenum addition was made for further solid-solution strengthening [2,3,4].

The efficiency of power plants could be improved by enhancing the steam parameter. At present, heat-resistant steels for the high-steam parameter of 650 °C are being developed. This has put heat-resistant steels such as T/P91, T/P92 and E211 out of consideration because of the loss of the microstructure stability during service at the high temperature [5-8]. More advanced steels should be developed to meet this requirement. It is well accepted in heat-resistant steels that highly stable microstructure will produce excellent creep strength. The precipitates are basically $M_{23}C_6$ and MX, and the MX-type carbides show much better stability than the $M_{23}C_6$ type carbide. In order to achieve microstructure with high stability, stable precipitates such as MX-type carbides are expected in heat resistant steels [8-12].

The aim of the present investigations was to study the influence of tempering temperature on microstructure previously normalized steels, one commercial 10CrMo9-10 steel and second the new experimental 15HM2 heat-resistant steel which contains more alloying contents relative to T22 (2¼Cr-1Mo) and other high-quality heat-resistant steels.

In the present study attention was paid to a much more detailed delineation of carbide morphologies formed in association with bainitic ferrite in two steels tested in the normalized-and-tempered (bainitic microstructure) conditions.

MATERIALS

The chemical compositions of the commercial 10CrMo9-10 and experimental 15HM2 steels are listed in Table 1 and the critical A_1, A_3, B_S and M_S temperatures are shown in Table 2.

Table 1. *Chemical compositions of the 10CrMo9-10 and 15HM2 steels used in this study*

Steel		C	Si	Cr	Mn	Mo
10CrMo9-10	wt.%	0.11	0.32	2.20	0.55	1.00
	%at.×10^2	0.51	0.63	2.35	0.56	0.58
15HM2	wt.%	0.14	0.23	0.88	0.73	2.4
	%at.×10^2	0.65	0.46	0.95	0.73	1.39

Table 2. *A_1, A_3, B_S and M_S temperatures*

Steel	Experimentally determined, °C					Calculated, °C	
	A_{c_1}	A_{c_3}	A_{r_1}	A_{r_3}	M_S	M_S	B_S
10CrMo9-10	780	875	-	-	-	433	532
15HM2	793	941	771	914	467	445	574

EXPERIMENTAL PROCEDURES

In order to establish the A_1 and A_3 temperatures (Table 2) dilatometric analysis was carried out on a Leitz-Wetzlar vacuum dilatometer using a 20 mm long by 3.5 mm diameter specimens. Adamel Lhomargy LK-02 high-speed dilatometer was used to establish the M_S temperatures (Table 2). In order to ensure rapid quenching (300 Ks^{-1}) the specimens were 12 mm in length and 1.0 mm in diameter.

Optical microscopy was used to examine etched structures. Microscopic images were recorded using the inverted metallographic microscope Nikon MA100 equipped with the ERC5s digital camera and the ZEN 2011 archiving program. Specimens were etched in 2% nital solution. The specimens for transmission electron microscopy (TEM) were machined to 3 mm diameter rods and subsequently were sliced into 0.35 mm thick discs while being kerosene cooled. The discs were subsequently ground down to a thickness of 40-50 μm. These specimens were finally electropolished in a twin-jet at room temperature and at 55-60 V using a 25-pct glycerol, 5 pct perchloric acid and 70 pct ethanol mixture. Thin foils were stored in ethanol and examined in a Tesla BS-540 transmission electron microscope at an operating voltage of 120 kV.

Quantitative *X*-ray analysis was used to determine the retained austenite content especially after normalizing. For this purpose, samples were examined in diffractometer operated at 38 kV and 10 mA using Fe-filtered CoK_α radiation. The retained austenite content was calculated from the *X*-ray intensities. A peak separation technique was used to separate the $(111)_\gamma$ -reflection from the overlapping $(110)_\alpha$ -reflection. Retained austenite was determined by method of direct comparison (Averbach-Cohen method) using the formula:

$$V_\gamma = \frac{C\frac{I_\gamma}{I_\alpha}}{1 + C\frac{I_\gamma}{I_\alpha}} \tag{1}$$

where:
I_γ – intensity of (111) austenite line,
I_α - intensity of (110) α phase line

$$C = \left(\frac{1}{v^2} F^2 p(L_p) e^{-2m}\right)_\alpha : \left(\frac{1}{v^2} F^2 p(L_p) e^{-2m}\right)_\gamma \tag{2}$$

where
v - atomic volume of unit cell,
F - structure factor,
P - multiplicity factor,
e^{-2m}- temperature factor,
L_p - Lorentz-polarisation factor

Vickers HV30 hardness measurements were performed according to PN-EN ISO 6507-1 on the Duramin Z-500 hardness tester.

RESULTS AND DISCUSSION

Volume fraction of retained austenite after normalizing followed by tempering at 500 and 550°C is presented in Fig. 1.

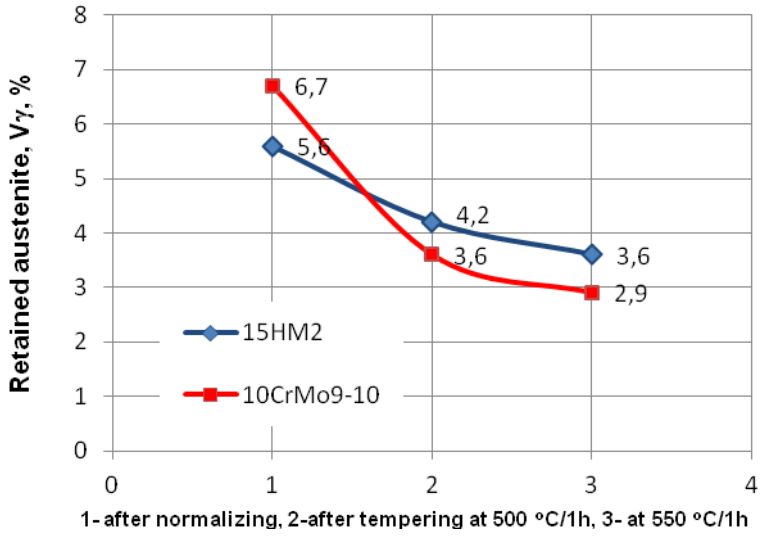

Fig. 1. Volume fraction of retained austenite after normalizing and tempering at 500 and 550°C

The measured hardness change after normalizing and tempering of 10CrMo9-10 and 15HM2 steels is shown in Fig. 2 for different tempering temperatures.

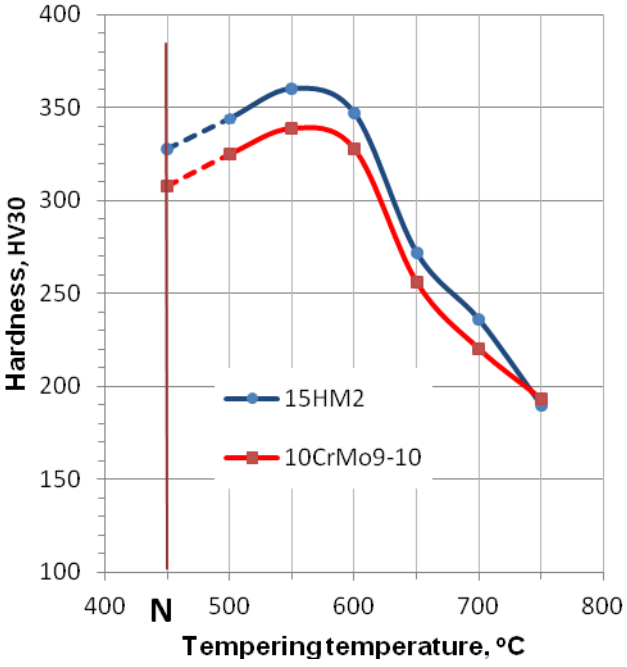

Fig. 2. Hardness change (HV30) after normalizing and tempering of 10CrMo9-10 and 15HM2 steels (N-means hardness after normalizing)

PHASE DIAGRAMS

The determined carbon concentrations of the residual austenite at the different temperatures of bainite transformations are compared with the T_0, T_0', A'_3 and A''_3, phase boundaries for investigated steels. It is usually assumed that the point where the bainitic microstructure ceases to change represents full transformation. But in case of bainitic transformation, reaction ceases before the parent phase (austenite) has completely transformed. It means that at any temperature below B_S and in the absence of any interfering secondary reactions only a limited quantity of bainitic ferrite forms before the reaction terminates [13, 14].

The calculated details for phase diagrams of the 10CrMo9-10 and 15HM2 steels and the carbon concentrations in austenite, x_γ at selected temperatures are shown in Tables 3 and 4.

Table 3. *Calculated details for phase diagram of the 10CrMo9-10 steel and the carbon concentration in austenite, x_γ at selected temperatures*

Transformation temperature, °C 10CrMo9-10	A_3',($x^{\gamma\alpha}$) mol	A_3'',($x^{\gamma\alpha}$ + 50J) mol	x_{To} mol	$x_{To'}$ mol	x_γ mol
510	0.0800	0.0767	0.0225	0.0117	0.0223
492	0.0862	0.0834	0.0242	0.0137	0.0210
481	0.0909	0.0879	0.0254	0.0150	0.0251
460	0.0955	0.0966	0.0273	0.0177	0.0254
445	0.1056	0.1029	0.0295	0.0196	0.0287

A_3' - $x^{\gamma\alpha}$ - paraequilibrium carbon concentration of austenite in mole fraction,

A_3'' - $x^{\gamma\alpha}$ + 50J - paraequilibrium carbon concentration of austenite in mole fraction but allowing for the 50J/mol stored energy,

x_{T_0} - T-zero carbon concentration in mole fraction,

$x_{T'_0}$ - the same but allowing for the 400J/mol stored energy.

The carbon concentration in austenite, x_γ, was determined as detailed elsewhere [15] by dilatometry. All details of the determination of carbon content in residual austenite are described elsewhere [15,16]. The obtained results in the area of these issues were discussed in a separate publication [16].

Table 4. *Calculated details for phase diagram of the 15HM2 steel and the carbon concentration in austenite, x_γ at selected temperatures*

Transformation temperature, °C, 15HM2	A_3', ($x^{\gamma\alpha}$) mol	A_3'', ($x^{\gamma\alpha}$ + 50J) mol	x_{To} mol	$x_{TO'}$ mol	x_γ mol
700	0.0233	0.0183	0.008	-	-
600	0.0520	0.0479	0.0157	0.0033	-
510	0.0840	0.0809	0.0243	0.0135	0.0076
500	0.0878	0.0848	0.0253	0.0147	0.0079
490	0.0918	0.0888	0.0261	0.0160	0.0121
475	0.0978	0.0950	0.0277	0.0179	0.0146
464	0.1023	0.0995	0.0293	0.0194	0.0162
400	0.1257	0.1235	0.0384	0.0267	-

In presented diagrams (Fig. 3 and 4) the bainitic reaction is found to stop when the average carbon concentration of the untransformed austenite is close to the T_0 and T_0' lines (black circles in Fig. 3 and Fig. 4) and supports formation of bainitic ferrite by a shear mechanism, since diffusionless transformation is not possible beyond the T_0 or T_0' curves.

The diagrams were calculated as in Ref. [17-18] using a model developed by Bhadeshia [19] based on the McLellan and Dunn quasi-chemical thermodynamic model [20]. The martensite and bainite reaction starts temperatures M_S and B_S were also marked on this diagrams. The paraequilibrium phase boundary is chosen because no substitutional alloying element partitioning occurs during bainite formation. In presented diagrams the reaction is found to stop when the average carbon concentration of the residual austenite is closer to the T_0' curve than the A'_3 boundary. The presented results can be explained when it is assumed that bainitic ferrite grows without diffusion, but any excess of carbon is soon afterwards rejected into the residual austenite by diffusion [21-23].

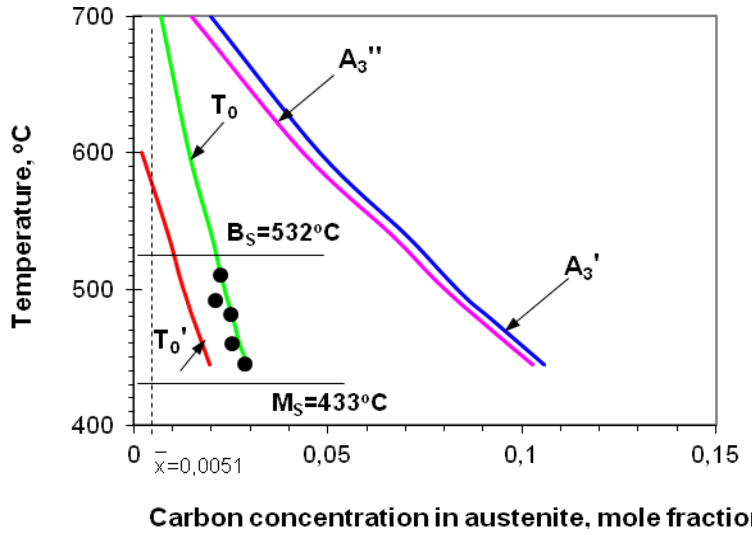

Fig. 3. The calculated phase boundaries A_3', A_3'', T_0 and T_0' for the investigated 10CrMo9-10 steel together with all the experimental data of the measured carbon contents of the untransformed austenite (black circles)

This makes more difficult for subsequent bainitic ferrite to grow, when the austenite becomes stabilised by increased carbon concentration. The maximum extent to which the bainite reaction can proceed is therefore determined by the composition of the residual austenite. A stage where diffusionless growth becomes thermodynamically impossible and the formation of bainitic ferrite terminates is where the carbon concentration of the austenite reaches the T_0' or T_0 curves.

If on the other hand, the ferrite grows with an equilibrium carbon concentration, then the transformation should cease when the austenite carbon concentration reaches the A'_3 curve [24-26].

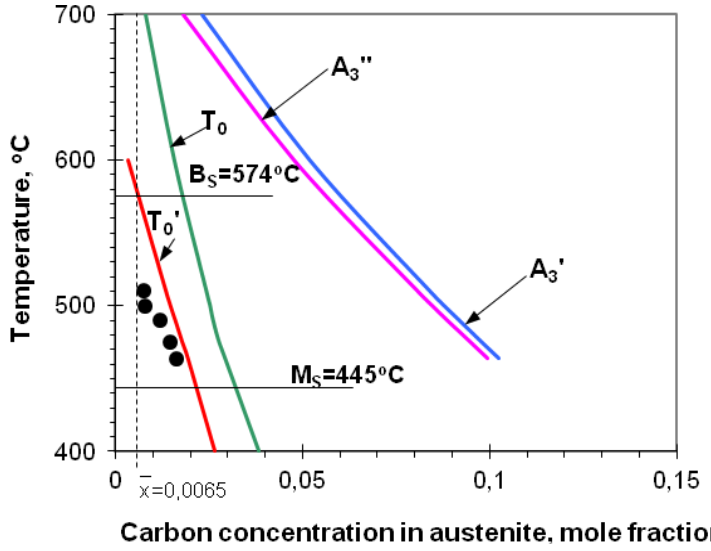

Fig. 4. The calculated phase boundaries A_3', A_3'', T_0 and T_0' for the investigated 15HM2 steel together with all the experimental data of the measured carbon contents of the untransformed austenite (black circles)

Thus, it is found experimentally that the transformation to bainite in both studied steels does indeed stop close to the T_0 boundary (Fig. 3 and 4) and the analysis suggest that bainite grows by displacive mechanism of transformation, but carbon atoms partition into residual austenite shortly after growth is terminated. Similar results have previously obtained by Bhadeshia and Christian [14] and by Ławrynowicz and Barbacki for other alloys [16, 27-29].

MICROSTRUCTURAL ANALYSIS

Light optical microscopy and transmission electron microscopy micrographs of the investigated steels were taken on the normalized and tempered condition. The microstructure of the 10CrMo9-10 steel is shown in Figures 5-9 while the 15HM2 steel microstructure is shown in Figures 10-14.

It was found that for both 10CrMo9-10 and 15HM2 steels the volume fraction of retained austenite decreased with increasing the tempering temperature (Fig. 1). The volume fraction of retained austenite after tempering above 600°C was beneath the level of resolution of applied X-ray diffractometer.

Microstructure of typical bainite after normalizing of the commercial 10CrMo9-10 and experimental15HM2 steels are seen in Fig. 5 and Fig. 10 respectively. The morphology of the bainite is similar to low carbon lath martensite, where dislocated laths are separated by films of retained austenite. Careful examination of this microstructure shows no evidence of carbides precipitation. This structure, therefore, belongs to upper bainite assuming that upper bainite in this steel is a structure composed of carbide free bainitic laths with interlath retained austenite films [13-16]. Retained austenite pools and films exist between the shaves and ferrite laths. Because carbides were not observed in the ferrite it probably means that the excess carbon in these ferrite laths partitions into the residual austenite soon after the growth event. The isolated films of austenite can accumulate carbon concentration close to T_0 line (Fig. 3). Because the austenite is greatly enriched in carbon they cannot transform to bainite

once the T_0 line is exceeded. Furthermore, these thin films of the residual austenite are stable to martensitic transformation on cooling to ambient temperature.

Figures 6 and 11 show microstructure obtained by normalizing and tempering at 500°C for 1hour. Transmission electron microscopy revealed that the sheaves were composed of much smaller laths of ferrite and the microstructure contain only bainitic ferrite and carbon enriched residual austenite films. Bainitic ferrite laths of thickness about 0.2÷0.3μm form separately one from another. Retained austenite was present between the ferrite laths as thin films. The ability to retain such films of austenite is due to partitioning of carbon into residual austenite following the formation of supersaturated bainitic ferrite. Carbides were difficult to observe in ferrite laths of thickness thinner than 0.3 μm. In this case films of residual austenite can accumulate all the excess carbon from supersaturated ferrite laths of thickness less than 0.3 μm. It is a possibility that, the carbon concentration of untransformed austenite is decreased by the carbide formation and then the reaction can proceed to a larger extent.

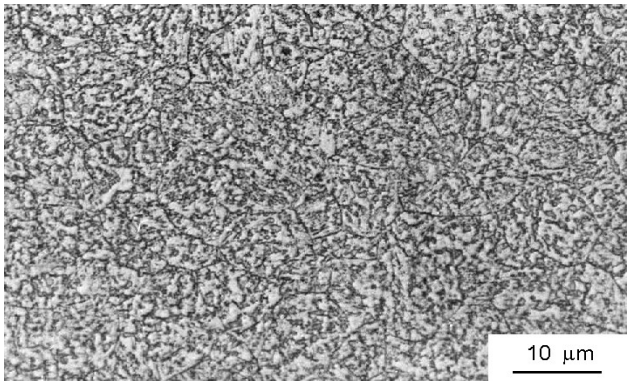

a)

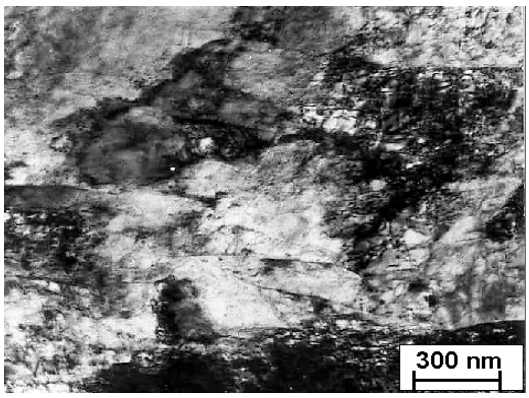

b)

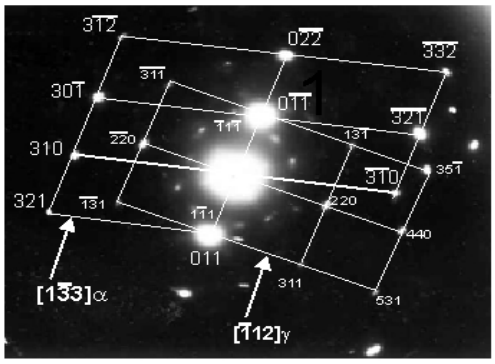

c)

Fig. 5. Microstructure of 10CrMo9-10 steel after normalizing, a) light microscopy, etched with 2% nital, b) TEM, thin foil, c) diffraction pattern with interpretation

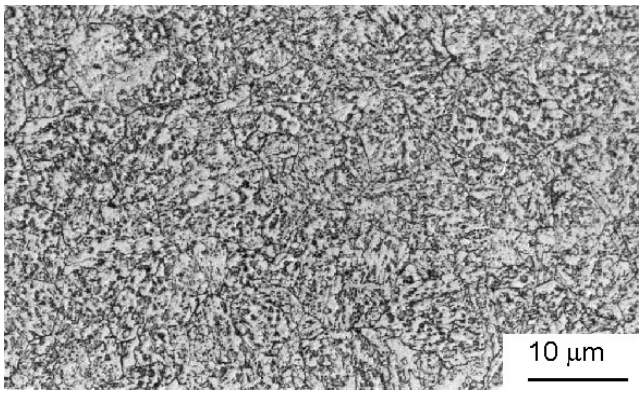

a)

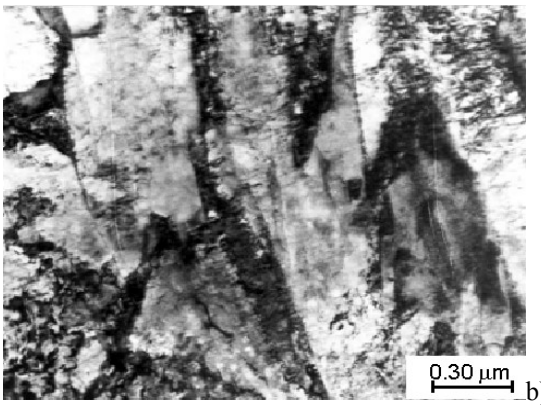

b)

Fig. 6. Microstructure of 10CrMo9-10 steel after normalizing and tempering at 500°C for 1h, a) light microscopy, etched with 2% nital, b) TEM, thin foil

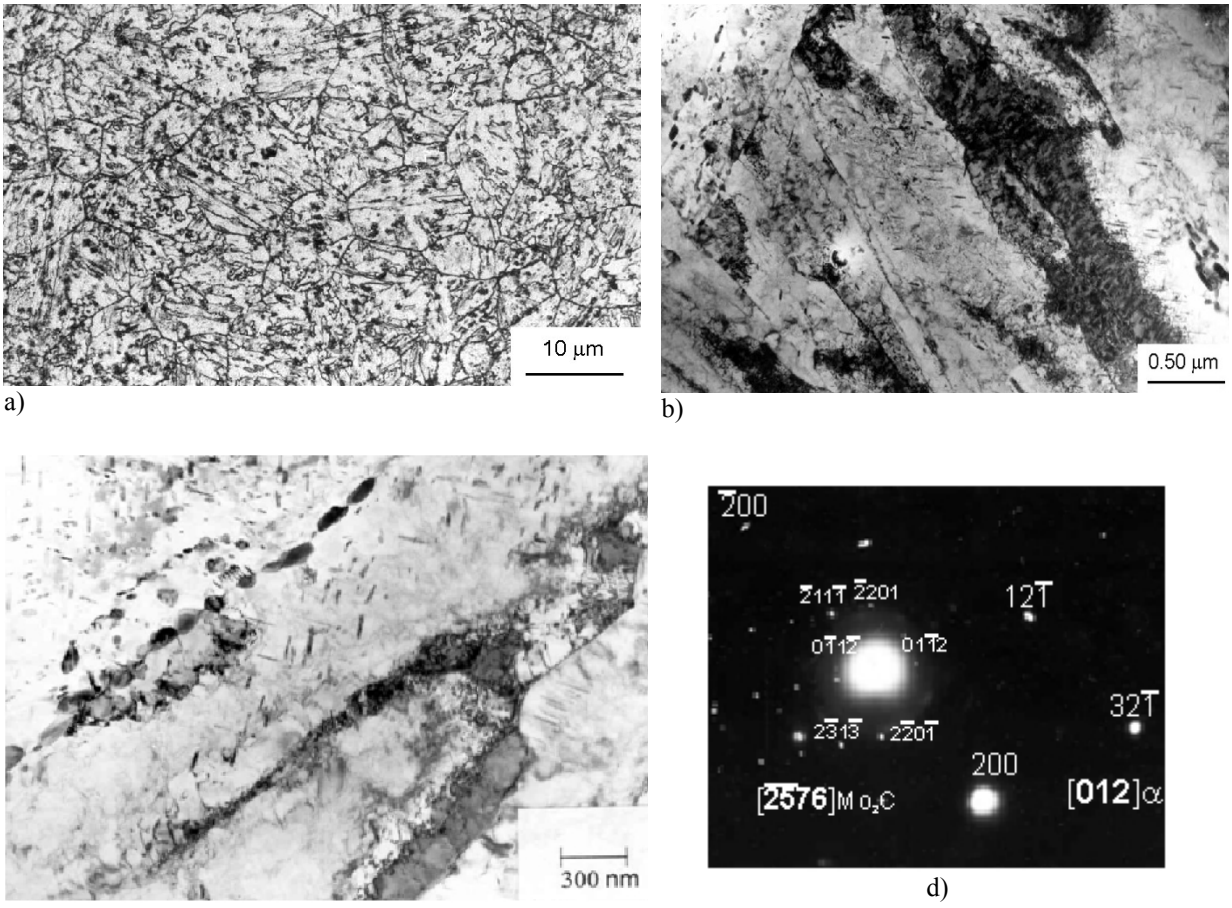

Fig. 7. Microstructure of 10CrMo9-10 steel after normalizing and tempering at 600°C for 1h, a) light microscopy, etched with 2% nital, b), c) TEM, thin foil, d) diffraction pattern with interpretation

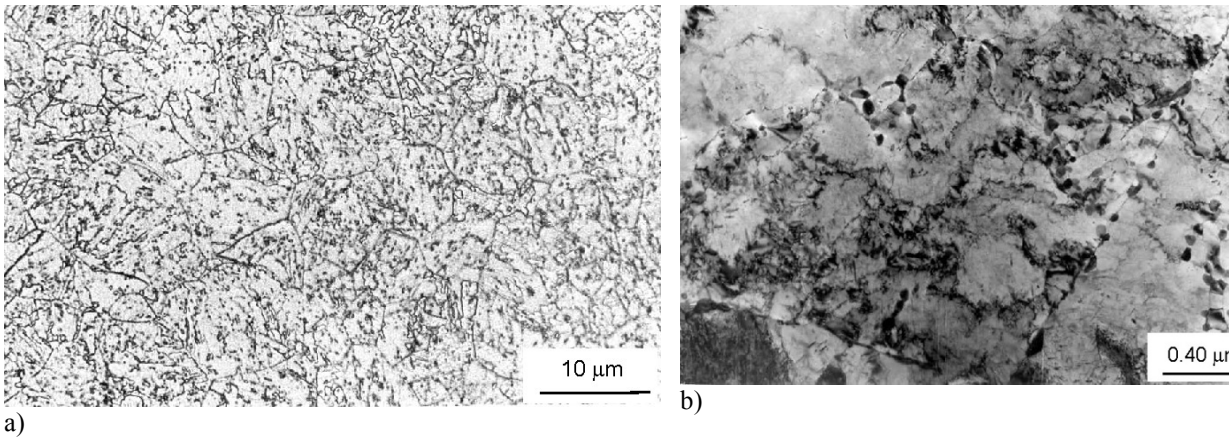

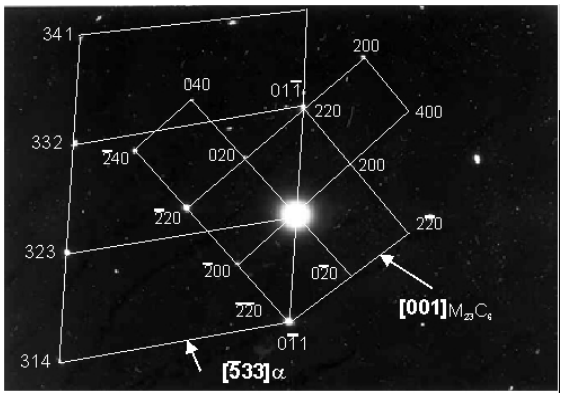

c)

Fig. 8. Microstructure of 10CrMo9-10 steel after normalizing and tempering at 700°C for 1h, a) light microscopy, etched with 2% nital, b) TEM, thin foil, c) diffraction pattern with interpretation

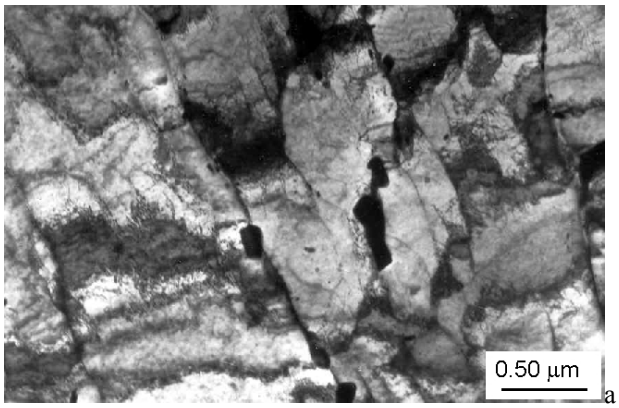

a)

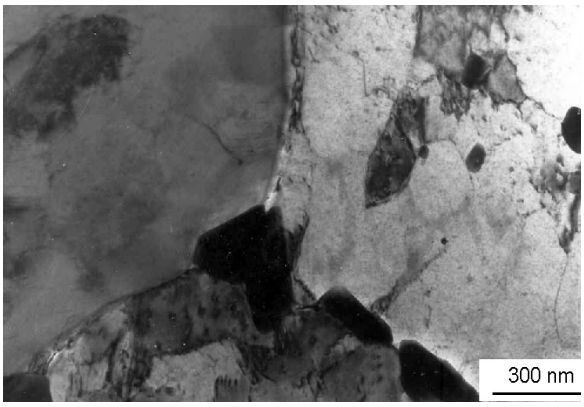

b)

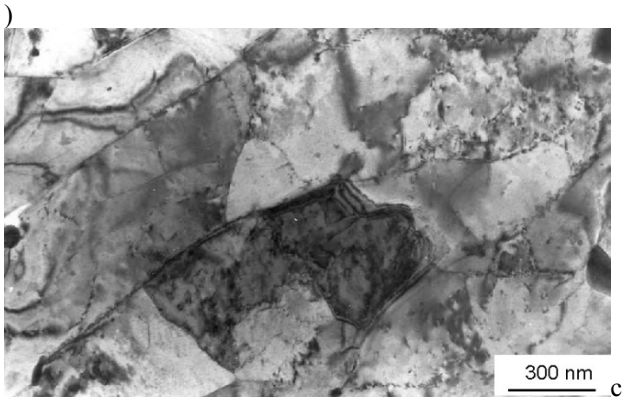

c)

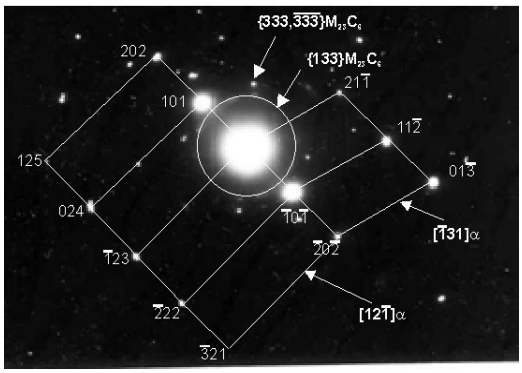

d)

Fig. 9. Microstructure of 10CrMo9-10 steel after normalizing and tempering at 750°C for 1h, a), b), c) TEM, thin foil, d) diffraction pattern with interpretation

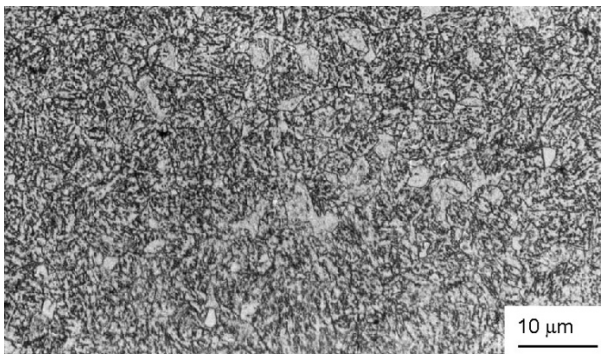

a)

b)

Fig. 10. Microstructure of 15HM2 steel after normalizing, a) light microscopy, etched with 2% nital, b) TEM, thin foil

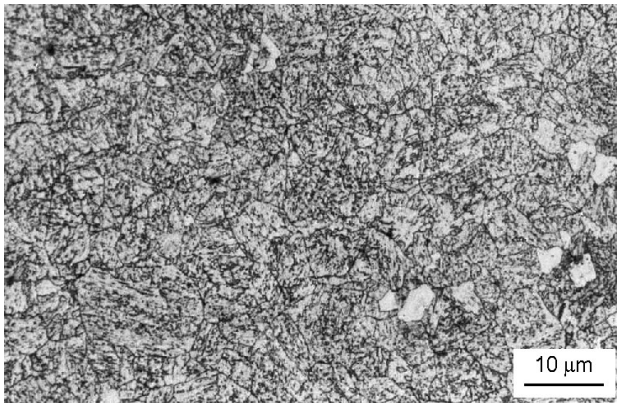

a)

b)

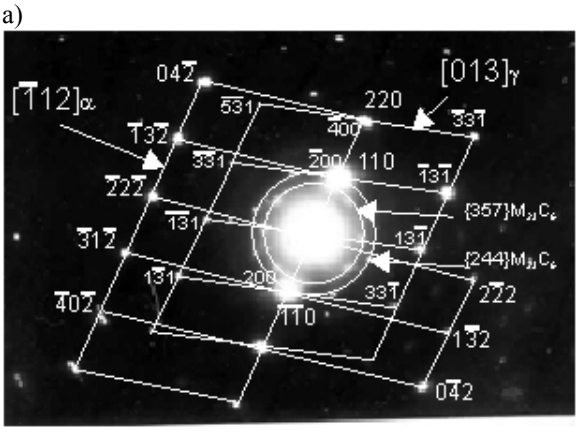

c)

Fig. 11. Microstructure of 15HM2 steel after normalizing and tempering at 500°C for 1h, a) light microscopy, etched with 2% nital, b) TEM, thin foil, c) diffraction pattern with interpretation

a)

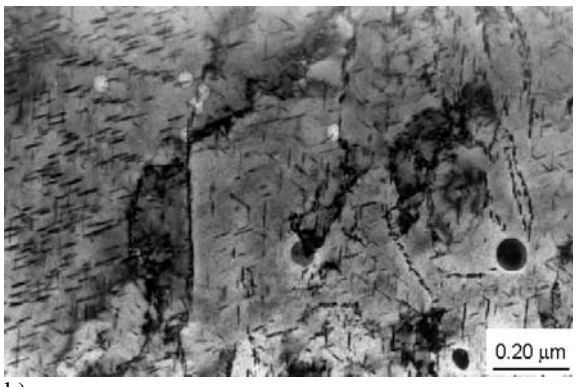

b)

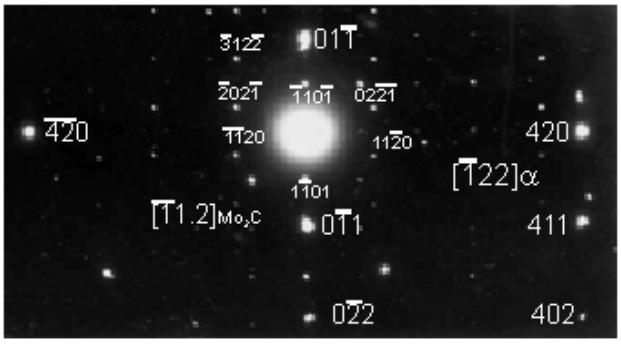

c)

Fig. 12. Microstructure of 15HM2 steel after normalizing and tempering at 600°C for 1h, a) light microscopy, etched with 2% nital, b) TEM, thin foil, c) diffraction pattern with interpretation

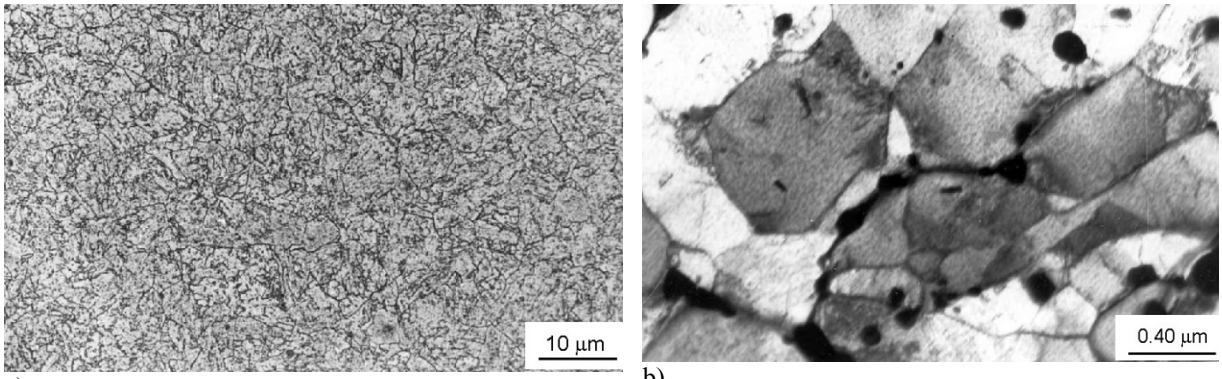

Fig. 13. Microstructure of 15HM2 steel after normalizing and tempering at 700°C for 1h, a) light microscopy, etched with 2% nital, b) TEM, thin foil

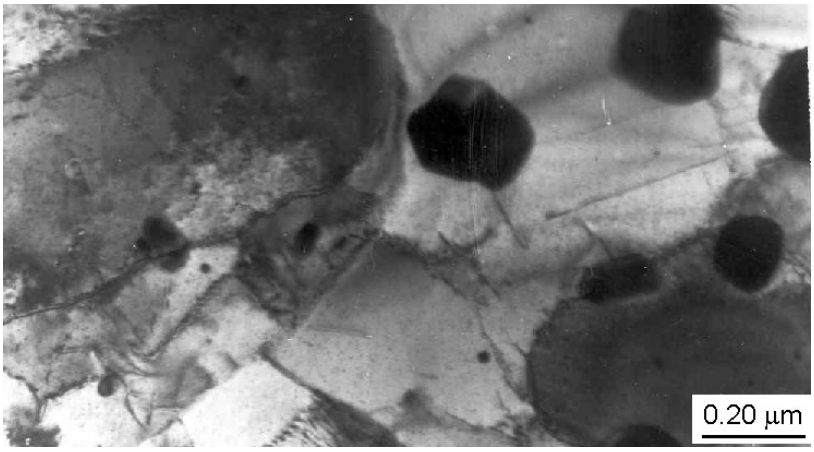

Fig. 14. Microstructure of 15HM2 steel after normalizing and tempering at 750°C for 1h, TEM, thin foil

The hardness of the steels is sensitive to changes in tempering temperature. With tempering at 500 and 550 °C, the hardness of the steels grows slightly compared to the hardness after normalization (Fig. 2). This shows that the way to strengthen the steels is mainly precipitate strengthening. The precipitation behavior of carbides is certain to affect the mechanical properties. The hardness of the steels shows normal response to the increasing tempering temperature above 550 °C, i.e. the hardness decreases with the increase of tempering temperature.

It is known that the formation of precipitates consumes dislocations. The carbide precipitation will decrease much the number of dislocations in the matrix, resulting in weakening of dislocation strengthening. On the other hand, the formation of carbides consumer the dissolved carbon, Cr and Mo which would provide a strong solid solution strengthening. Therefore, although the carbide precipitation could produce precipitation strengthening, it is not enough to compensate for the loss of dislocation strengthening and carbon, Cr and Mo solid solution strengthening.

When the tempering temperature is increased, a large amount of carbides form in the matrix. When the steel is heated at 600 °C, a small amount of precipitates form on the lath of the bainitic ferrite and on the prior austenite grain boundaries and a certain amount of precipitates has formed in the matrix (Fig. 7 and Fig. 12). The indexing of the diffraction patterns in Figures 7d and 12c indicates that these carbides are M_2C. When the tempering temperature is raised to the fastest precipitation temperature, precipitation is not only in the grain boundary and lath boundaries, but also a large number of precipitates form in the lath

interior. At this time, there is a large increase in the total precipitation amount. Precipitation hardening is the main mechanism of steel strengthening, impacting on the tempered bainite hardness. Changes in the hardness with tempering temperature essentially reflect changes of the amount, size and distribution of carbide precipitation in the matrix phase.

The hardness rapidly decreases with increasing tempering temperature, especially when tempered above 600 °C After tempering at higher temperatures, e.g. 600 °C and over, the lattice distortion in bainitic structure and the dislocation density are greatly reduced. So, when the tempering temperature rises, the changes in these strengthening factors in the matrix are small, while there will be major changes in the number, size and distribution of the precipitates in the matrix. The higher the tempering temperature, the stronger the diffusion capacity of carbon atoms. The nucleation of carbides in the matrix is fast. A greater number of finer size precipitates can be obtained, with more uniform distribution. Such precipitation is extremely beneficial, for increasing hardness and toughness of the material. However, large amounts of precipitates consume a lot of carbon atoms, greatly reducing the solid solution strengthening effect in bainitic matrix, but also thereby imparting better matrix ductility.

When the steels are heated to 700 and 750 °C, compared to the steels heated to 500 and 600 °C, the number of precipitates in the microstructure within the bainitic ferrite laths and on grain boundaries increases significantly (Fig. 8 and Fig. 13). The carbide phase grows to a large size in a relatively short tempering time (1hour). The increasing amount of carbide phase could decrease the solid solution strengthening effect due to the consumption of dissolved Cr and Mo atoms. The distribution is denser, and depicts the prior austenite grain boundaries. Also, precipitates have greater size and dispersed distribution in the microstructure of steel, and are not linked together. In the steel heated to 700 and 750°C, the precipitates $M_{23}C_6$ are larger in size. A large number of precipitates are distributed along the grain boundaries, outlining the contours of the grain boundaries (Fig. 9 and Fig. 14). The size of precipitates on the grain boundary is significantly larger than the size of the precipitate inside the grain. The microstructural morphology is the typical structure of tempered 2¼Cr-1Mo bainitic steel.

CONCLUSIONS

1. It is found experimentally that the transformation to bainite in both studied steels stop close to the T_0 boundary and the analysis suggest that bainite grows by displacive mechanism of transformation but carbon atoms partition into residual austenite shortly after growth is terminated.

2. Tempering at elevated-temperatures (500-550^{o}C) previously normalized steels causes a hardness increase mainly by precipitate strengthening. Tempering at higher temperatures (600-750^{o}C) causes reduction in the dislocation density and polygonization of bainitic ferrite, previously normalized steels which is reflected in the hardness reduction. Along with the reduction in dislocation density, the $M_{23}C_6$ particles coarsen, allowing the bainitic ferrite laths to transform to more equiaxed subgrains. Along with the coarsening of the $M_{23}C_6$, there is also a coarsening in the M_2X precipitate distribution, although these particles coarsen much more slowly than $M_{23}C_6$.

REFERENCES

1. Zheng-Fei Hu, Heat-Resistant Steels, Microstructure Evolution and Life Assessment in Power Plants. Thermal Power Plants. Dr. Mohammad Rasul (Ed.), ISBN: 978-953-307-952-3. (2012) 1-266. Available from: http://www.intechopen.com/books/thermal-power-plants/heat-resistant-steels-microstructure-evolution-and-lifeassessment-in-power-plants.

2. Klueh R. L., Elevated-temperature ferritic and martensitic steels and their application to future nuclear reactors. November 2004. Metals and Ceramics Division, OAK RIDGE NATIONAL LABORATORY, Oak Ridge, Tennessee, ORNL/TM-2004/176. 1-56.

3. Motagi B.S., Ramesh Bhosle, Effect of Heat Treatment on Microstructure and Mechanical Properties of Medium Carbon Steel. International Journal of Engineering Research and Development, 2, 1 (2012), 7-13.

4. Zieliński A., Golański G., Sroka M., Influence of long-term ageing on the microstructure and mechanical properties of T24 steel, Materials Science & Engineering A, 682 (2017) 664–672.

5. Dobrzanski J ., Hernas A., Moskal G., Microstructural degradation in boiler steels: materials developments, properties and assessment. Woodhead Publishing Limited. Chapter 6 (2011) 222-271.

6. Dziuba-Kałuża M., Zieliński A., Dobrzański J., Sroka M.: The evaluation of suitability for operation of low-alloy Cr-Mo and Cr-Mo-V steel welded joints beyond the design work time. Archives of Materials Science and Engineering, 66 1 (2014), 21-30.

7. Sroka M., Zieliński A., Mikuła J., The service life of the repair welded joint of Cr-Mo / Cr-Mo-V. Arch. Metall. Mater., 61 3 (2016), 1315–1320.

8. Zieliński A., Miczka M., Boryczko B., Sroka M.: Forecasting in the presence of microstructural changes for the case of P91 steel after long-term ageing. Archives of Civil and Mechanical Engineering, 16 (2016), 813-824.

9. Jingjie Shen, Huilong Yang, Yanfen Li, Sho Kano, Yoshitaka Matsukawa, Yuhki Satoh, Hiroaki Abe: Microstructural stability of an as-fabricated 12Cr-ODS steel under elevated-temperature annealing. Journal of Alloys and Compounds, 695 (2017), 1946-1955.

10. Shrestha T., Alsagabi S.F., Charit I., Potirniche G.P, Glazoff M. V., Effect of Heat Treatment on Microstructure and Hardness of Grade 91 Steel. Metals, 5 (2015), 131-149.

11. Kumari R., Das G., Effect of Isothermal Ageing on Microstructure and Mechanical Behavior of 0.5Cr-0.5Mo-0.2V Low Alloy Steel. Journal of Materials & Metallurgical Engineering, 5 3 (2015), 7-14.

12. Taylor Roth Jacobs, Elevated temperature mechanical properties of line pipe steels, A thesis submitted to the Faculty and the Board of Trustees of the Colorado School of Mines in partial fulfillment of the requirements for the degree of Masters of Science (Metallurgical and Materials Engineering).

13. Aaronson H.I., Reynolds W.T., Shiflet G.J., Spanos G., Bainite Viewed Three Different Ways. Metall. Trans. A 21A, (1990), 1343-1380.

14. Bhadeshia H.K.D.H., Christian J.W., Bainite in steels. Metall Trans. A, 21A (1990), 767–797.

15. Ławrynowicz Z., Mechanism of bainite transformation in Fe-Cr-Mo-V-Ti-C steel. International Journal of Engineering, 12 (1999), 81-86.

16. Ławrynowicz Z., Barbacki A., Features of Bainite Transformation in Steels. Advances in Materials Science, 2 (2002), 5-32.

17. Bhadeshia H.K.D.H., David S.A., Vitek J.M. and Reed R.W., Stress induced transformation to bainite in Fe-Cr-Mo-C pressure vessel steel. Materials Science and Technology, 7 (1991), 686-698.

18. Dyson D.J., Holmes, B., Effect of alloying additions on the lattice parameter of austenite. J. Iron Steel Inst., 208 (1970), 469-474.

19. Bhadeshia H.K.D.H., Bainite in steels 2nd ed., London, The Institute of Materials, (2001).

20. McLellan, R.B., Dunn, W.W., J.Phys.Chem. Solids., 30 (1969), 2631-2637.

21. Ławrynowicz Z., Ausferritic or Bainitic Transformation in ADI, Proceedings of the 12th International Symposium on Advanced Materials, Paper No: 98, Rawalpindi, Pakistan, ISAM 2011.

22. Ławrynowicz Z.: Affect of cementite precipitation on the extend of bainite transformation in Fe-Cr-C steel. Advances in Materials Science. 11 (2011), 13-19.

23. Ławrynowicz Z., Decarburisation of bainitic ferrite laths and its influence on the microstructure in Fe-Cr-Si-C steel. Advances in Materials Science, 11 2 (2011), 56-64.

24. Hehemann R.F., Kinsman K.R., Aaronson H.I., A debate on the bainite reaction. Metall. Trans., 3 (1972), 1077–1094.

25. Ławrynowicz Z., Affect of decarburisation times of bainitic ferrite laths on the microstructure in Fe-Cr-C steel. Journal of Polish CIMAC, 6 (2011), 127-136.

26. Caballero, F.G., Miller, M.K., Babu, S.S., Garcia-Mateo, C., Atomic scale observations of bainite transformation in a high carbon high silicon steel, Acta Materialia, 55 (2007), 381-390.

27. Ławrynowicz Z., Carbon Partitioning During Bainite Transformation in Low Alloy Steels, Materials Science and Technology, 18 11 (2002), 1322-1324.

28. Ławrynowicz Z., Transition from Upper to Lower Bainite i Fe-C-Cr Steel, Materials Science and Technology, 20 11 (2004), 1447-1454.

29. Ławrynowicz Z., Próba wykorzystania mechanizmu przemiany bainitycznej do modelowania kinetyki i mikrostruktury stali niskostopowych (The attempt of the using of the bainite transformation mechanism to modelling of kinetics and microstructure of the low alloy steels), Wyd. Uczelniane UTP Bydgoszcz, Rozprawy Nr 137, 2009.